Prediction, analysis and design for indoor climate in large enclosures

Shuzo Murakami
Institute of Industrial Science, University of Tokyo
Tokyo, Japan

Summary

Design methods and prediction techniques for indoor climate of a large enclosure are described. The difficulties of environmental control peculiar to large enclosures are discussed in terms of capacity, height of ceiling and small occupied zone, etc. The basic principles for designing ventilation, heating, and cooling are noted. Next, three prediction methods for indoor climate in a large enclosure, i.e. empirical equations, scale model tests and numerical simulations, are outlined. In particular, the difficulties in using numerical simulation for large enclosures are clarified. Lastly, some case studies of numerical simulation of large enclosures are introduced.

Prediction, analysis and design for indoor climate in large enclosures

Shuzo Murakami
Institute of Industrial Science, University of Tokyo
Tokyo, Japan

1. Introduction – progressive enclosure and control of outer space

In recent years, such various types of large- scale enclosures as atria, domes, and auditoriums have become quite common and often function as symbols of their cities.

Environmental control of these large enclosures is much different and more difficult than for such smaller spaces as offices. The designing methods and prediction techniques for indoor climate peculiar to such large enclosures are described in this paper.

Historically, the construction of large enclosures has been necessitated by the demand for ever larger interior space. The evolution of environmental control technology can be divided into the following four stages:

Stage 1) simple enclosure of outdoor events (protection from rain, wind, and solar rays);
Stage 2) simple change from outdoor to indoor climate (ventilation);
Stage 3) high level environmental control of large enclosure (heating, cooling);
Stage 4) complete enclosure of a city (cf. Figure 3).

We are presently in stage 3, while stage 4 awaits future developments.

The demand for a comfortable environment has risen year by year, and accordingly techniques for environmental control have also become evermore sophisticated in order to fulfill that demand. The major purpose of this paper is to review the state of the art of environmental control for large enclosures at the level of stage 3 listed above.

Figure 1 compares the plans of various large enclosures and structures. As is shown here, there exist many large enclosures with various scales and shapes. Figure 2 illustrates in cross section the scale of large enclosures in comparison with other types of large structures.

The future or fourth stage of large enclosures as projected in Japan is shown in Figure 3 [1~3]. These huge scale structures are designed to accommodate about 100,000 inhabitants in one building and to function as "indoor cities". Feasibility studies are now in progress, but I think that realization of the original plans is questionable, considering such matters as cost and present technological levels.

2. Prime characteristics of large enclosures determining indoor climate

The expression "large enclosures", as used in the context of environmental control, does not mean simply a large indoor space. Here, this phrase is intended to highlight the difficulty of proper environmental control in large indoor spaces. These difficulties are closely related to the scale and shape of such spaces, and to the usual seating arrangement in which the zone occupied by people is located near the floor of the structure. Some of the major elements used to define a "large enclosure" from the view point of indoor climate control are 1) the height of the ceiling, 2) the capacity of the space, and 3) the small region for human occupancy near the floor.

(1) Height of ceiling

Where the ceiling is very high, a large vertical temperature distribution is likely to occur. The major difficulties in designing heating and cooling systems for a large enclosure are caused by this unavoidable temperature distribution in such spaces. In other words, no matter how wide a space is, any space with a low ceiling does not fall within the category of "large enclosures" as used here.

(2) Capacity of space

In large enclosures, it is often difficult to arrange supply and exhaust openings in suitable positions. Furthermore, interior heat sources are often distributed very unevenly. Therefore large distributions of temperature and air velocity are likely to occur not only in the vertical direction but also in the horizontal direction.

(3) Zone occupied by people

In large enclosures, the region occupied by people is usually limited to the lower region of the total space. The area of this zone occupied by people is, in general, extremely small in comparison to the total capacity of the entire enclosure. Furthermore, office spaces are sometimes open to large-scale indoor open spaces (cf. Figures 7, 26~31). In these cases, the overall indoor climate control of both the large enclosure and the office spaces is very difficult.

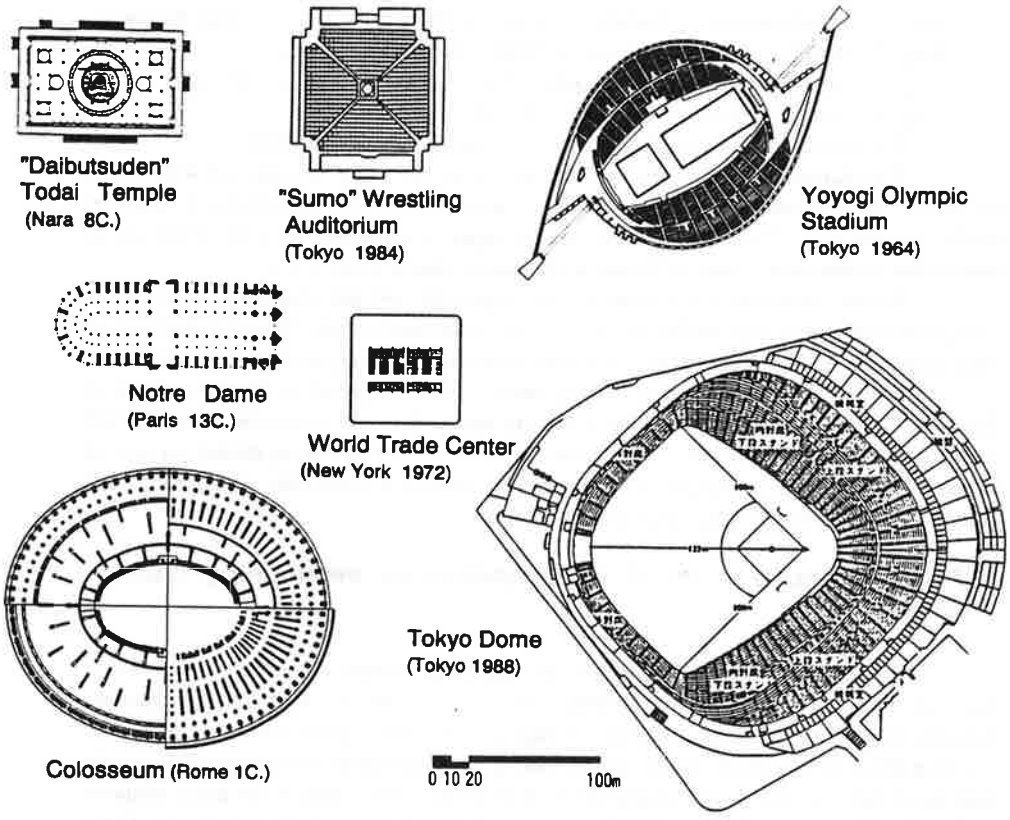

Fig.1 Plans of various large enclosures and large structures

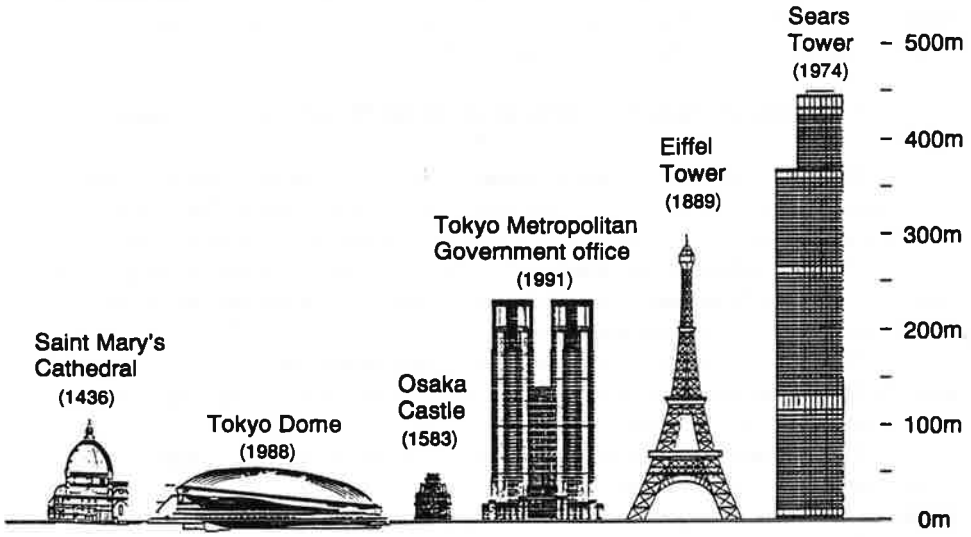

Fig.2 Cross section of various large structures

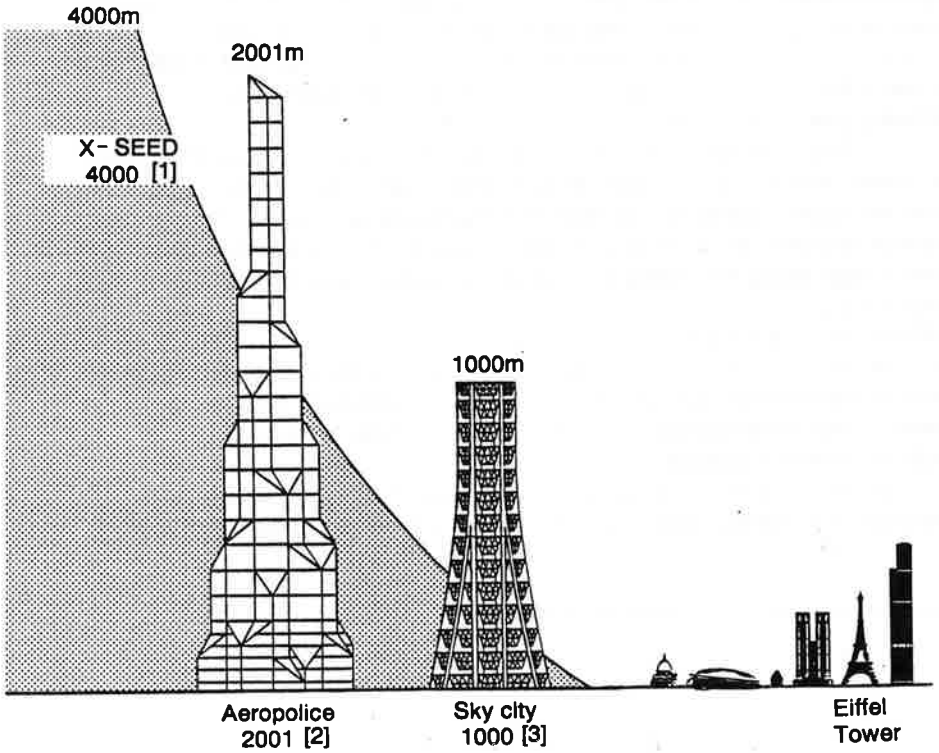

Fig.3 Projects for super structures in Japan

(4) Outer wall

Walls and ceilings (or roofs) of large enclosures usually face directly to the outside. The ratio of outer to inner surface in large enclosures is much larger than that for usual office spaces. In this case, the indoor climate is almost certain to be affected by the outdoor climate, which makes fine control of the indoor climate very difficult.

3. Keys to proper control of indoor climate of large enclosures

Indoor climate designs of large enclosures are very diverse and change according to the purpose of the structure and the number of people to be accommodated. The zone occupied by people and their density also vary in accord with the function, and these factors also directly influence the heat load for air-conditioning. In the case of indoor stadiums, there are further special environmental requirements since, for example, even minor wind currents may influence performance in such sports as rhythmic gymnastics.

From the view point of energy-efficient environmental control, the most important goal is to limit the air-conditioned regions to the occupied zone near the floor, which is always a tiny proportion of the total space.

There are thus the following obstacles to be overcome in designing a well-controlled indoor climate for a large enclosure.

(1) Difficulty related to shape

Since the ceiling is high, a large temperature distribution in the vertical direction is likely to occur. Furthermore, the potential locations for supply and exhaust openings are usually greatly limited, so these are often arranged in undesirable positions. These unsuitable arrangements of supply openings consequently often require a large air volume and a long travel distance for the supply jet, and this in turn often gives rise to a temperature distribution in the horizontal direction and hence complaints about cold drafts are likely to occur.

(2) Difficulty given by structure

The long-span structural system of large enclosures often influences the design of indoor climate control. In particular, because of the need to decrease the weight of the structure, the thermal capacity and insulation of roofs, ceilings and walls is often insufficient even though these surfaces usually face the outside directly. This lack of thermal insulation necessitates large heating and cooling loads and also gives rise to cold drafts along the ceiling and walls in winter.

(3) Difficulty due to utilization

The ratio of occupied space to total available space is small, hence the zone which should be air-conditioned is also limited to a small area. Furthermore, the usage, the number of persons, and the time of utilization may also change greatly from day to day.

(4) Difficulty related to capacity

The air change rate is usually small in such spaces because of their huge capacity. Consequently air movement is suppressed, often giving rise to a strong thermal stratification.

4.Principles for designing ventilation, heating and cooling systems for a large enclosure

(1) Ventilation design

When designing ventilation for a large enclosure, the passive method should be examined first of all, since the air volume to be ventilated is huge. The passive method consists of so-called natural ventilation, i.e. wind-induced or buoyancy-induced. Active methods should be applied only to areas found difficult to control merely by the passive method. A combination of passive and active control is essential.

(2) Cooling design

The basic principle is to cool the least possible area required by the specific function of the structure. In small spaces such as offices, full cooling is usual; however, in large enclosures, it is necessary to cool only the small occupied region near the floor. The cooling design goals for these two types of enclosure are compared in Figure 4. In a large enclosure, it is most effective to design for minimum diffusion of the cold air, which will naturally accumulate at the bottom of a space because of its own physical property. Therefore, in the design stage, it is important to predict the trajectory of the supply jet and to select proper positions for the supply and exhaust openings, focusing on the target zone to be cooled. The rate of descent of the cold jet due to negative buoyancy is unexpectedly large.

Since the zone to be cooled is usually located in a lower region, it is usually very effective to blow cold air at a low velocity, allowing the cool air to accumulate at the bottom of a large enclosure. In this case, the temperature remains very high in the upper part of the enclosure. Although there thus exists a large temperature distribution in the vertical direction, the occupied zone is maintained at a comfortable temperature.

Figure 5 illustrates the cooling design goals for the Tokyo Gymnasium (Tokyo Japan, 1990), which follows the principles stated above. Figure 6 is a visualization of air movement given by a field experiment. The pooling of cold air at the bottom is well illustrated here.

When the zone to be cooled is located in a higher position, effective cooling is more difficult. In this case, it is important to properly set the supply opening so that the target zone is attacked directly by the jet and covered in cold air. An example of this design principle is shown in figure 7. Hot air, it should be remembered, remains naturally in the uppermost region.

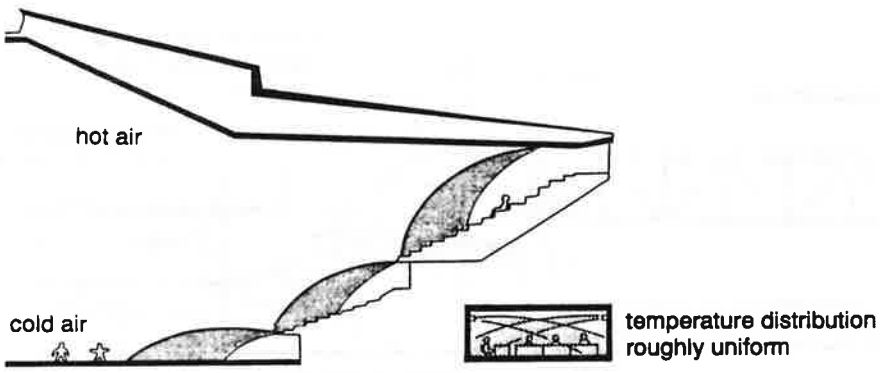

Fig. 4 Cooling designs for large and small enclosures

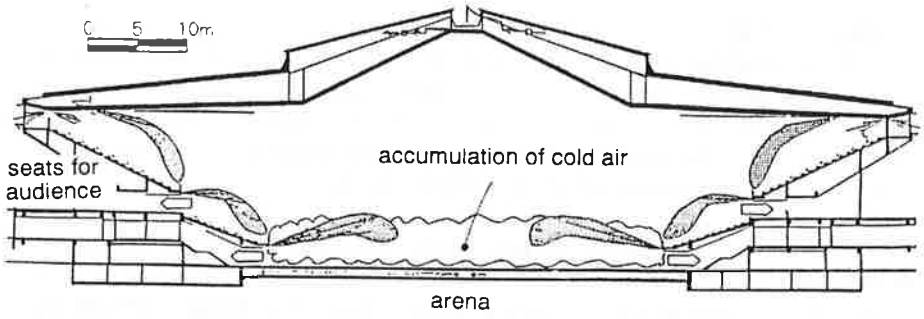

Fig. 5 Cooling design policy for Tokyo Gymnasium (Tokyo, Japan)

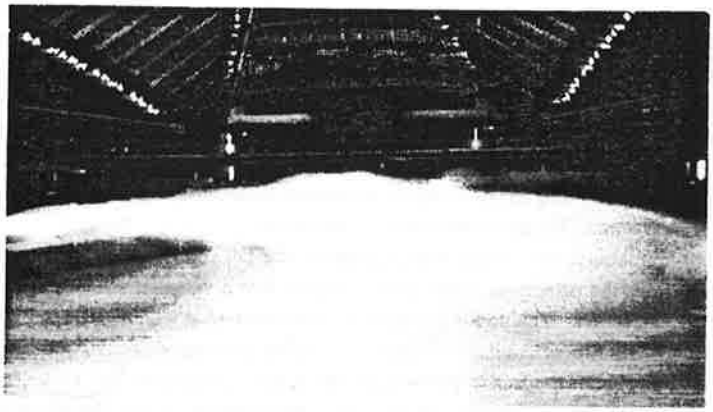

Fig. 6 Visualization of air movement given by field experiment (cooling, at Tokyo Gymnasium)

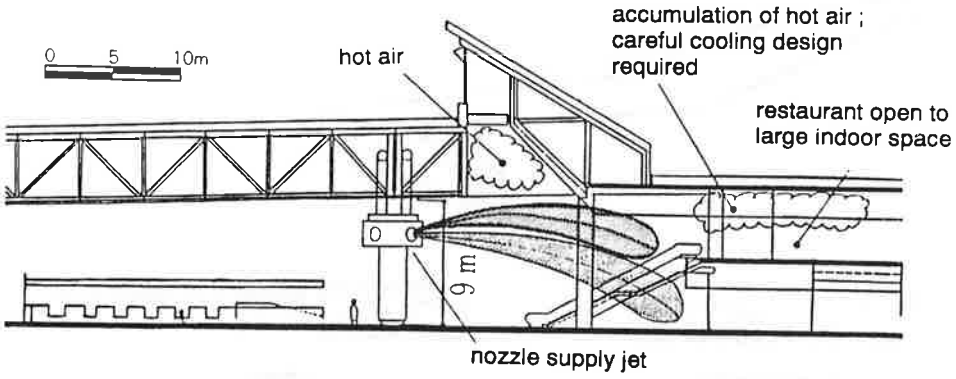

Fig. 7 Spot cooling focused on particular area (air terminal building)

(3) Heating design

In contrast to cool air, warm air rises due to buoyancy. As figure 8 indicates, warm air rises and stays just beneath the ceiling where there are no people. A flow visualization of warm air given by a field test at Tokyo Gymnasium (figure 9) shows very clearly the rising of warm air, which makes heating the occupied zone near the floor very difficult.

The most reliable heating system in a large enclosure is thus to supply warm air directly to the target zone, using floor heating or air supply openings under the seats. An example of the latter method of spot heating is shown in Figure 10. If such partial heating systems are insufficient or difficult to use, it is necessary to provide fan-systems which mix and circulate warm air within the entire enclosure. Such systems are able to carry warm air to the bottom of an enclosure. Figure 11 illustrates the system used at Osaka-Jo Hall (Osaka, Japan, 1983), where high-speed nozzles set in the ceiling carry warm air to the occupied zone below [4] :

1) warm air is mixed with cold air by high-speed nozzles set in the ceiling;
2) exhaust openings are set at arena level, i.e. at the bottom of the enclosure.

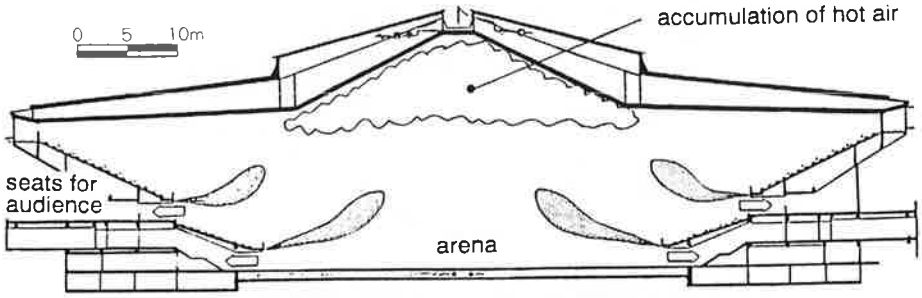

Fig. 8 Movement of supplied hot air

Fig. 9 Visualization of air movement given by field experiment (heating, at Tokyo Gymnasium)

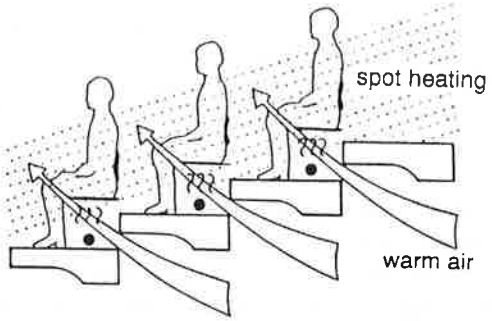

Fig. 10 Air supply openings under seats (heating)

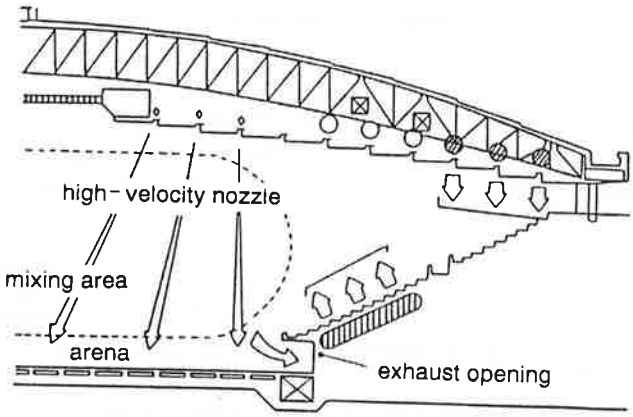

Fig. 11 Mixing by high-speed nozzle at ceiling and exhaust opening at arena level
(Osaka-Jo Hall, Osaka, Japan,1983)

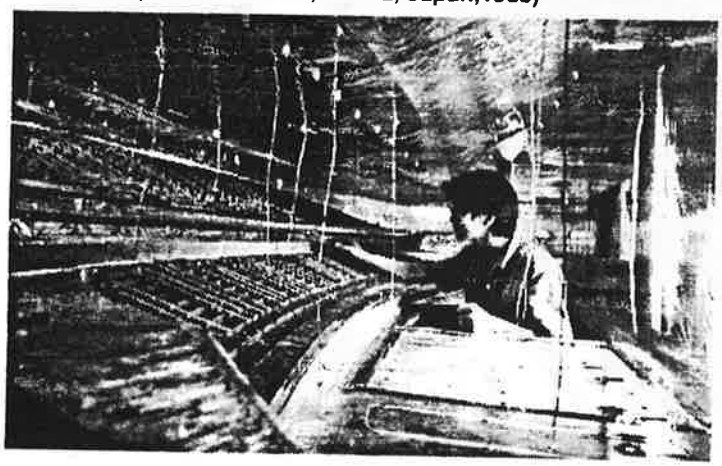

Fig. 12 Inside view of 1/20 scale model of Tokyo Gymnasium

The latter arrangement is fundamental to proper heating design in a large enclosure. It is also effective to use radiant heating.

When the thermal insulation of roof, ceiling and walls is poor, cooling in those areas is likely to cause down- drafts. These drafts, which often create large circulation flows encompassing the total space, act to reduce the large vertical temperature distribution.

5. Prediction methods for indoor climate of large enclosure

When designing the indoor climate of a large enclosure, the preliminary examination is most important. There are three well known methods:

1) prediction of trajectory of supply jet;
2) scale model experiment;
3) numerical simulation.

5.1. Prediction of trajectory of supply jet

Empirical equations, such as eq.(1), are used to predict the trajectory of the jet, giving the center- line values of the velocity and the temperature of the supply jet [5].

$$Z/D_0 = \pm 0.42 \cdot (\beta \cdot g \cdot \Delta T_0 \cdot D_0 / (K \cdot V_0^2)) \cdot (X/D_0)^3 \qquad (1)$$

X, Z : travelling length of jet in horizontal and vertical directions
ΔT_0: initial temperature difference of jet
V_0: initial velocity of jet
D_0: equivalent diameter of opening

This method is most popular since it is very simple and practical.

However, such empirical equations are originally formulated on the basis of the movement of a jet in an isothermal free space. When applied to the movement of a jet in a closed space, such equations often give large errors because the movement of the supply jet is significantly affected by the surrounding air temperature and the surrounding walls.

5.2. Scale model experiment

A scale model test is one of the most effective methods for predicting the temperature and air velocity distributions in large enclosures. Although very expensive and tedious to perform, scale model tests have often been conducted in many countries, since before the development of numerical simulation, it was the only reliable prediction method. Figure 12 shows the inside of a 1/20 scale model of Tokyo Gymnasium [6]. When conducting a scale model test, similarity conditions should be properly considered. The important similarity conditions are as follows;

1) sufficiently large Reynolds number for the room air flow to be turbulent;
2) similarity for Archimedes number for supply jet etc.;
3) similarity for heat flux (convective and radiative) at wall boundary etc.

The physical process of heat transfer concerned with indoor climate is shown in Figure 13 [6]. Similarity laws are deduced by modelling these processes by mathematical equations. When planning a scale model test, we must decide the scope of the environmental region to be simulated. Figure 14 shows three possible levels of modelling. Experiments based on level 1 modelling are most popular [6].

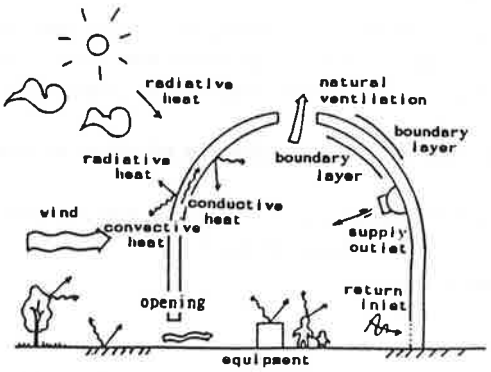

- Indoor climate composed of many complex physical processes.
- Similarity laws deduced exactly from similarity of governing equations and boundary conditions.
- In actual experiments exact similarity laws often relaxed for convenience of prosecution.

Fig. 13 Physical processes of heat transfer concerned with indoor climate

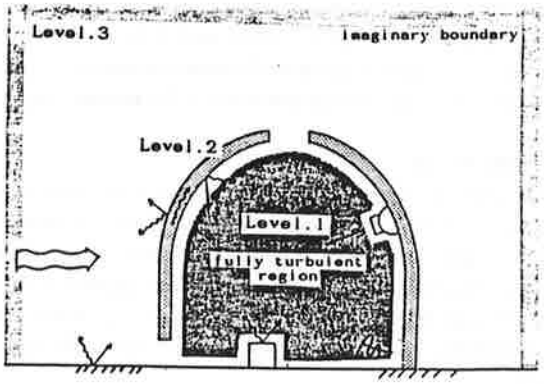

- Model testing may be classified into three levels.
  Level 1: indoor space only
  Level 2: indoor space with shelter
  Level 3: indoor space with surrounding outdoor environment

Fig. 14 Classification of simulated regions in model experiments

5.3. Numerical Simulation

In recent days, the method of predicting a non- isothermal turbulent flow field by numerical simulation has been greatly advanced. This has been supported by the development of both software and hardware. Many researchers and engineers have begun to use this technique for predicting the indoor climate of a large enclosure and have achieved many successes, as will be shown later. However there still exist many difficulties for predicting the indoor climate accurately, since the indoor climate of a large enclosure is very complicated, as will also be shown later. As this technique is still developing rapidly, such difficulties are certain to be overcome in the future. The details of designing a simulation system for a large enclosure will be described in the next section.

6. Design principles for numerical simulation of indoor climate in a large enclosure

6.1. Difficulties residing in the numerical simulation

There exist many difficulties in simulating the flow field of a large enclosure, and these are mainly caused by the following two factors:

1) the size of the space is large;
2) the flow field is very complicated.

When the space is large, we are forced to conduct a simulation with coarse dividing mesh. For example, if a large enclosure of 30m × 30m × 30m is discretized into small cells using a huge mesh system of 100 × 100 × 100 (=10^6), one side of the cell is still 30cm, which is quite large for simulating a turbulent flow field accurately.

The coarse meshes used in the simulations always caused various types of numerical errors, as will be discussed later. But since the use of a coarse mesh system is unavoidable when conducting a simulation of a large enclosure, we must design the total software system keeping in mind both the limitations of coarse discretization as well as the available computer resources. The most important point in simulation design is to balance the requisite prediction accuracy and the CPU resources needed to achieve that accuracy.

The complicated flowfield of a large enclosure is characterized by the following factors:

1) an elliptic flow composed of separation, reattachment, circulation etc.;
2) non- isotropic, highly three dimensional;
3) non- isothermal, strong thermal stratification.

Accurate prediction of such a turbulent flow field is very difficult. The well- known k- ε model often fails to give successful results in the simulation of such flow fields.

6.2. Choice of turbulence models

The well- known k- ε model has been used very widely, yielding many successful results in engineering applications. Originally the k- ε model was developed in the field of mechanical engineering for analyzing simple turbulent flows, e.g. channel flow or pipe flow etc. When the k- ε model is applied to such flows, it gives very accurate results. However, the k- ε model reveals some shortcomings when applied to a non- isotropic, non- isothermal flow field in a enclosure, since this model is based on simple isotropic eddy- viscosity modelling (EVM). Here I would like to show two examples.

Figure 15 shows the results of experiments and simulations concerned with the flow field around a building model [7]. Three turbulence models, k- ε , ASM (Algebraic stress model), LES (Large eddy simulation) are compared here. All models show similar results for

the velocity vectors, as shown in Figure 15 (1). However the small reverse flow on the roof is not reproduced in the result of k- ε , which is a very serious error although the area is very small. The reason k- ε produces this error can easily be understood by considering Figure 15 (2). In the case of k- ε , the value of turbulence energy k is overestimated greatly at the frontal corner. This large k value produces large eddy viscosity ν_t and thereby the reverse flow on the roof is negated by this large ν_t . The mechanism of this overestimation of k in the k- ε model is shown in Appendix 1. This overestimation of k at the impinging region is one fundamental shortcoming residing in EVM.

An analysis of a non- isothermal flow field in a enclosure is shown in Figure 16 [8]. The model of the enclosure used here has a cooling jet at the left side wall and a heated right side wall. Around the center line of the cooling jet appear some differences between the results of k- ε and ASM. The distributions of velocity and temperature around the center line are less steep in the case of ASM (cf. Figures 16 (2), (4)). It has been confirmed here that the results of ASM correspond better to the experiments than do those of k- ε . A remarkable difference is observed in the prediction of turbulent heat flux $\overline{u_i \theta}$, as is shown in Figures 16 (5), (6). The result of ASM is certainly more accurate than that of k- ε . The reason why such a large difference occurs is shown in Appendix 2. This failure of k- ε results from the utilization of EDM (eddy diffusivity modelling) and represents another serious shortcoming of this model. The relative abilities of various turbulence models are compared in Table 1.

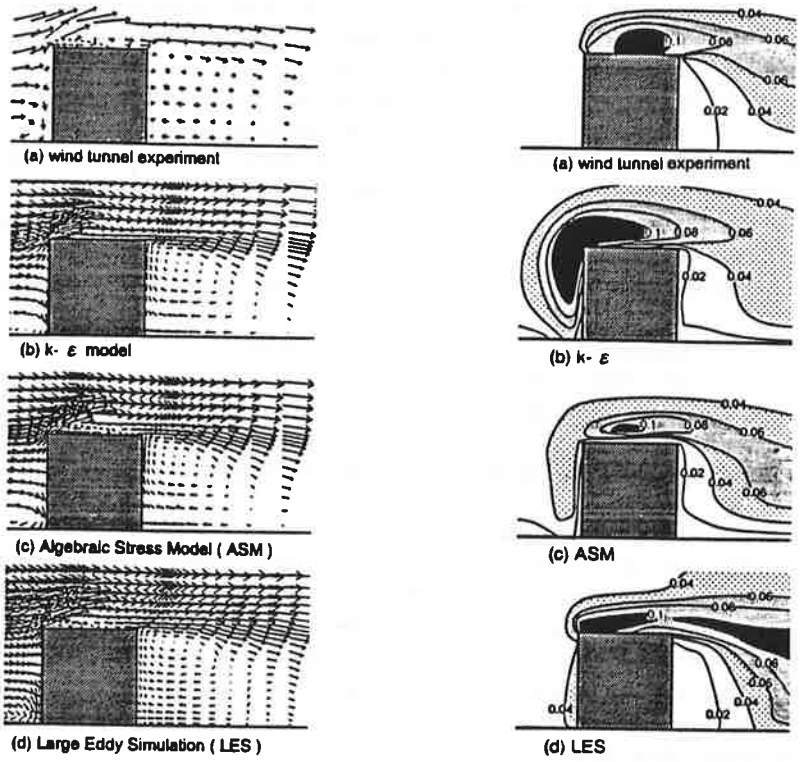

(1) velocity vector field **(2) turbulence energy k**

Fig. 15 Flow field and turbulence energy around building model (given by k- ε , ASM and LES)

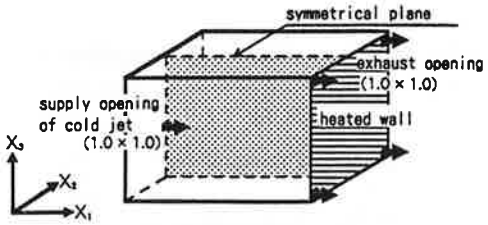

room model

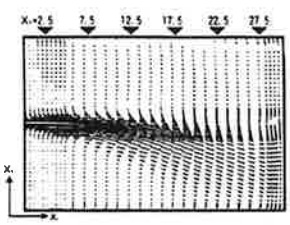

(1) velocity vector (ASM)

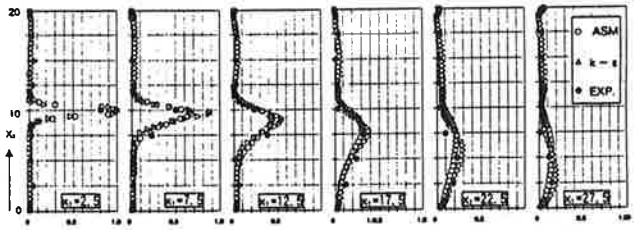

(2) scalar velocity (k- ε , ASM)

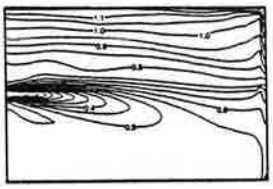

(3) temperature (ASM)

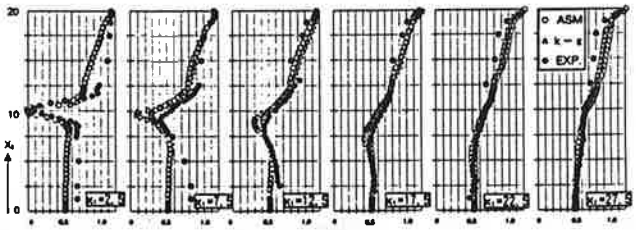

(4) temperature (k- ε , ASM)

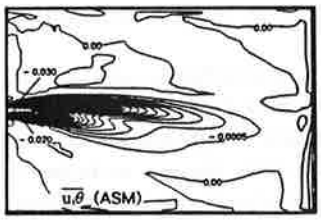

(5) turbulent heat flux $\overline{u_i \theta}$ (ASM)

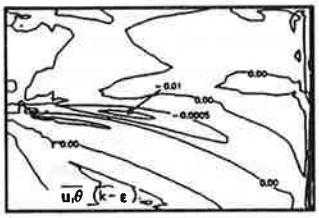

(6) turbulent heat flux $\overline{u_i \theta}$ (k- ε)

Fig. 16 Velocity and temperature fields in an enclosure

6.3. Grid discretization

As stated above, we are forced to conduct simulations of large enclosures using coarse grid discretization. Since such simulations cannot be entirely free from numerical errors caused by mesh coarseness, their relative degree of accuracy must be confirmed by experimental data. The values of solution errors are compared for two levels of mesh coarseness [9] in Figure 17; (1) shows the results using a coarse mesh system while in (2) the grid discretization becomes much finer, in particular at the corner of the building model. Solution error is reduced remarkably in Figure 17 (2).

The most important regions for simulation of a flow field in a enclosure are the areas

Table. 1 Relative comparison of various turbulence models for practical modelling of enclosure

Turbulence model / wall boundary condition	Standard k−ε wall function	Low-Re. No. k−ε non-slip	Standard DSM ASM wall function	Low-Re. No. DSM ASM non-slip	LES wall function	LES non-slip
1. Simple flows (channel flow, pipe flow, etc.) (local equilibrium is valid)	○	○	○	○	○	○
2. Flow with streamline curvature						
1) weak curvature, convection is dominant (usually observed in room)	○	○	○	○	○	○
2) strong curvature (flow around bluff body)	X , △	X , △	○	○	○	○
3. Jet						
1) normal	○	○	○	○	○	○
2) swirl	X	X	○	○	○	○
4. Impinging flow	X , △	X , △	○	○	○	○
5. Non − isothermal flow						
1) weak stratification	○	○	○	○	○	○
2) strong stratification	X , △	X , △	○	○	○	○
6. Convective heat transfer at wall	X , △	○	X , △	○	X , △	○
7. Flowfield with low Reynolds No.	X , △	△ , ○	X , △	△ , ○	○	○
8. Unsteady flow, unsteady diffusion						
1) highly unsteady	X	X	X	X	○	○
2) vortex shedding	X	△	△	○	○	○

○ : functions well △ : insufficiently functional X : functions poorly

The most important regions for simulation of a flow field in a enclosure are the areas around the supply jet and the exhaust opening, since the velocity gradient is very steep in these areas. Most energy production and dissipation is generated here. Therefore we should be very careful in setting the grid discretization in these areas. However, it is very difficult to discretize these areas finely when simulating a large enclosure and this may be the greatest difficulty in conducting simulations of large enclosures.

In Figure 18, the effect of grid discretization is examined for the area between two supply jets [10]. 4 grids are set in the area between the two jets in Figure 18 (1) but 8 grids are set in Figure 18 (2). In the case of the fine mesh system (Figure 18 (2)) a small rising stream is observed near the floor in the area between the two jets but it is not observed in the case of the coarse mesh (Figure 18 (1)). The existence of this small rising stream is confirmed by experiment.

In Figure 19, a rough analysis is conducted in the area of the supply jet itself [10]. In the case of Figure 19 (1), one side of the opening is divided into two grids, but 4 grids are used in the case of Figure 19(2).

There exists a steep velocity- gradient layer along the mixing layer which surrounds the core region of the supply jet. In the case of Figure 19 (4), two peaks of k value at these mixing layers are reproduced, while such peaks are omitted in the case of Figure 19 (3) and, rather, the whole area of the supply jet shows a large value of k. The distribution of k becomes very vague in the case of coarse mesh (cf. Figure 19 (3)).

In the analysis of large enclosures, it is usually impossible to arrange sufficiently fine grids at the supply and exhaust openings, so the simulation results will inevitably have significant errors in these regions.

The use of a composite grid system is effective in overcoming this difficulty. In this technique, fine mesh discretization is applied only in areas where the velocity gradient is very

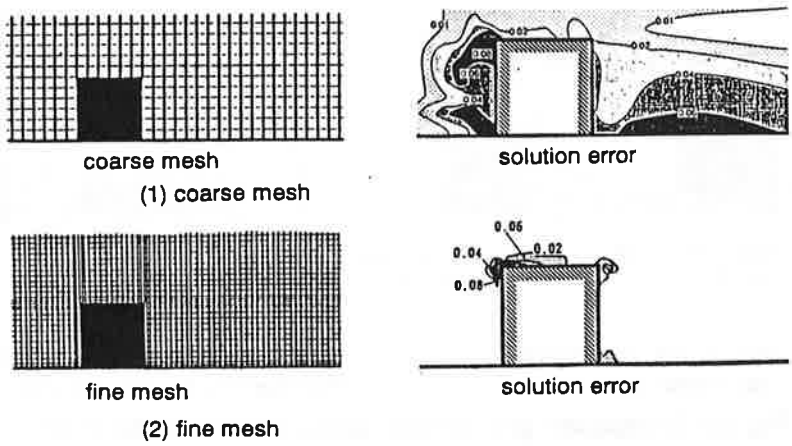

Fig. 17 Effect of grid discretization on solution error

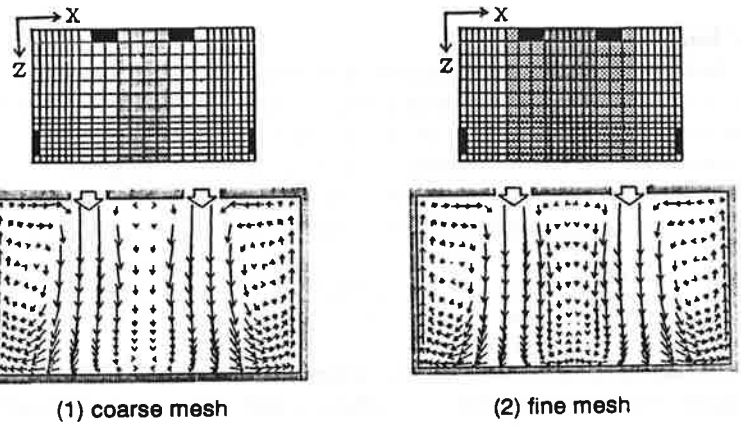

Fig. 18 Effect of grid discretization on flow field near the floor

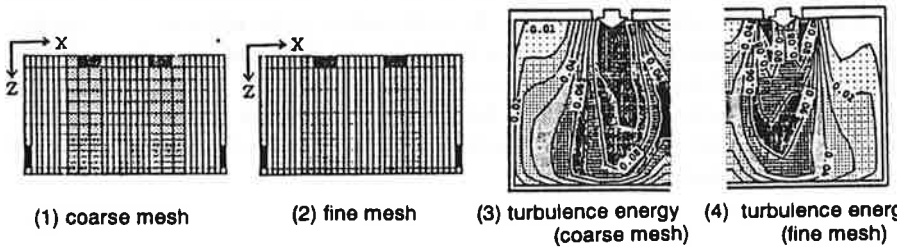

Fig. 19 Effect of grid discretization on turbulence energy k around supply jet

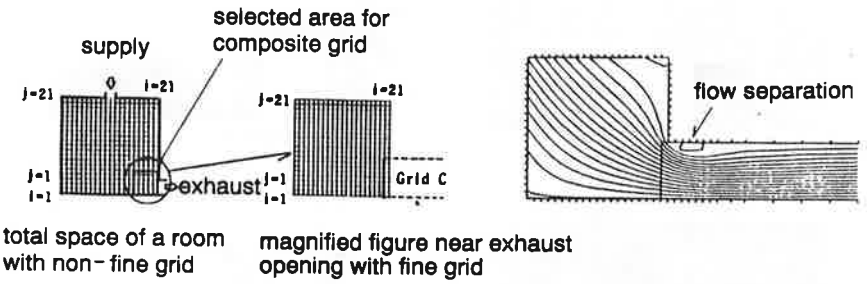

(1) Two regions for applying composite grid **(2) Stream line near exhaust opening (magnified area by composite grid)**

Fig. 20 Composite grid system applied for room air flow

steep, being careful to connect smoothly the fine grid zone and the coarse grid zone. Figure 20 illustrates an example of a composite grid system applied to an exhaust opening [11].

6.4. Wall boundary condition

The forced use of coarse discretization in the analysis of a large enclosure also creates difficulties in setting boundary conditions at a solid boundary. Even if we discretize the space with a huge mesh system on the order of 10^5~10^6, the value of wall unit y^+ ($y^+ = u^* y / \nu$) would still be around the order of 10~10^2. Therefore, it is usually difficult to use a non-slip boundary condition at a solid wall, and we are forced instead to use some type of wall function. The most popular one is the so-called generalized log law, shown below [12].

$$\frac{U_i}{(\tau_w/\rho)}(C_\mu^{1/2}\cdot k)^{1/2}=\frac{1}{\kappa}ln\left[\frac{E\cdot(h_i/2)\cdot(C_\mu^{1/2}\cdot k)^{1/2}}{\nu}\right] \qquad (2)$$

However, an examination of the basic assumption used to deduce this equation leads to the conclusion that it is not theoretically justifiable to apply this type of wall function to an area that includes flow separation, circulation and reattachment etc., which are usually observed in an enclosure. From this view-point, the development of a new wall function is highly desirable, one which can be applied more universally to the flow field within an enclosure.

The application of a wall function to a flow field in an enclosure sometimes fails to give accurate results. It is particularly limited in the analysis of the heat transfer mechanism at a wall. In such cases, we should use the Low-Reynolds number model with non-slip boundary condition. Unfortunately, application of this model to a 3D fully-turbulent flow with high Reynolds number will remain difficult because of limited CPU capacity. One way to overcome this difficulty is to approximate the flow field by a 2D model and then apply the Low-Reynolds number model with non-slip boundary condition, where the heat transfer at the wall can be analyzed accurately.

6.5. Case studies in the analysis of large enclosures

Three examples of numerical analyses for various types of large enclosures are introduced here.

6.5.1. Case study 1 ; analysis of airport terminal lobby (Kansai New Airport, Osaka, Japan, under construction) [13, 14]

In the initial stage of basic design for the airport terminal building, analysis was carried out on the departure lobby of the airport under various conditions (Murakami et al. 1990). The building model used for the analysis is shown in Figure 21. The structure consists of three areas: an atrium section, a central building section and an airside section.

1) Outline of numerical analysis (Figure 21)

The terminal building, which measures 300m x 150m, is comprised of 10 structures, each unit 30m long, connected in the longitudinal direction. Calculations were performed for a half span (15m) of one unit, taking advantage of the symmetry of this structure. The calculations were carried out for the arrangement of air inlets and outlets for air conditioning during the initial stage of basic design, as shown in Figure 21. The standard k- ε model was used here. Heat fluxes through the ceiling and floor were given as boundary conditions with respect to temperature. The size of the grid system was 72(X) × 15(Y) × 35(Z)=37800.

2) Results of numerical simulation under heating conditions (Figure 22, 23)

At the central section, the warm air blown out of a large nozzle (SP2) ascends due to the effect of buoyancy, creating a large recirculating flow covering the entire center area (Figure 22, center). Because of this air flow, the air in the central section was thoroughly mixed, and a roughly uniform temperature distribution(20 to 22 ℃) was obtained. In the atrium and the airside section, the air was well mixed (Figure 22) owing to the air supply opening on the floor (SP1) and the nozzle supply opening (SP6). The temperature distribution was uniform (Figure 23) compared with the case of cooling, which will be described later. However, the temperature at the floor level was relatively low (between 17 and 20℃).

3) Results of numerical simulation under cooling condition (Figure 24, 25)

The cold air from the large nozzle in the central section (SP2) and from the nozzle at the airside supply opening (SP6) descended due to its negative buoyancy (Figure 24). The temperature exceeded 45 ℃ near the ceiling and was approximately 23 ℃ near the floor, and

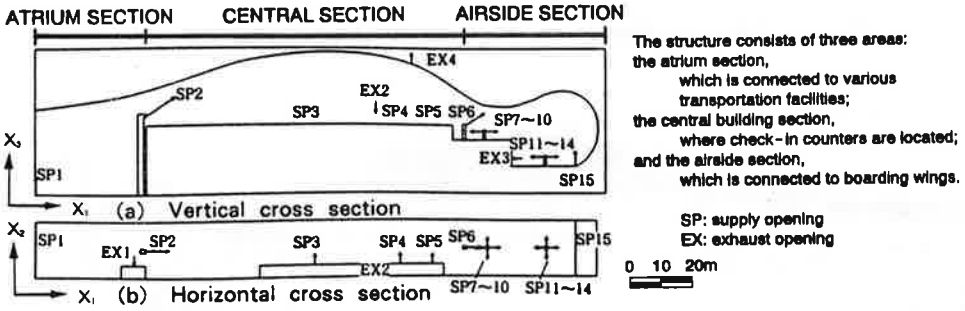

Fig. 21 Building model used for calculation
(air terminal lobby, Kansai New Airport, Osaka, Japan, under construction)

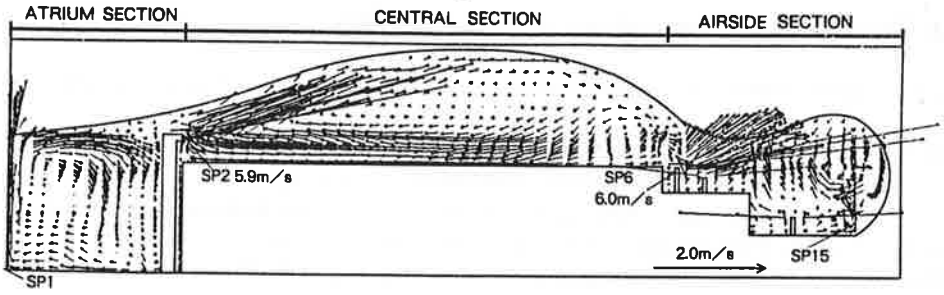

Fig. 22 Air flow distribution under heating condition
(vertical section at the center)

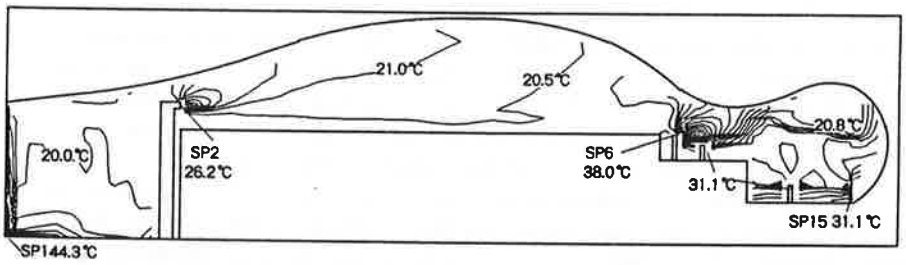

Fig. 23 Temperature distribution under heating condition

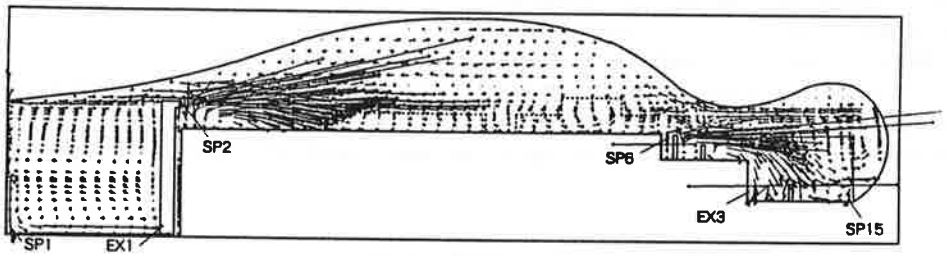

Fig. 24 Air flow distribution under cooling condition

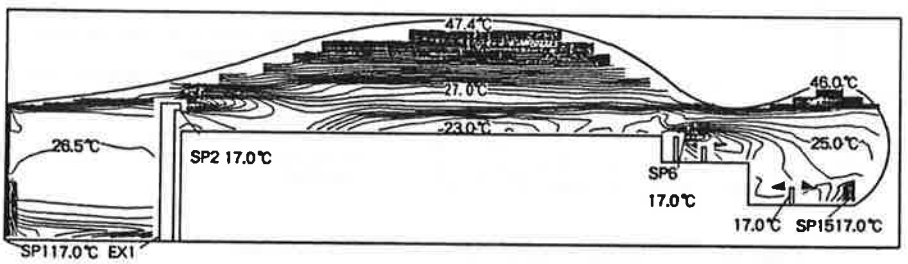

Fig. 25 Temperature distribution under cooling condition

the isothermal lines were distributed horizontally (thermal stratification). The temperature near the floor was within a moderate temperature range (between 22 and 27 ℃). Some other simulations under different conditions were conducted to determine proper arrangement of air supply and exhaust openings.

6.5.2. Case study 2 ; analysis of atrium sandwiched between two structures [14]

The configuration of the building used is shown in Figure 26. The building is laid out with the offices located on the south and north wings of the building and the atrium sandwiched between them. In summer, the temperature is very high in the upper region of the atrium, and it was feared that the air temperature of the offices on the upper floors would also become high because of heat penetration from the atrium. In order to avoid this undesirable situation, an 8m - high storage space for hot air was arranged at the top of the atrium. In this study, a numerical analysis was carried out under cooling conditions, with attention paid to the following:

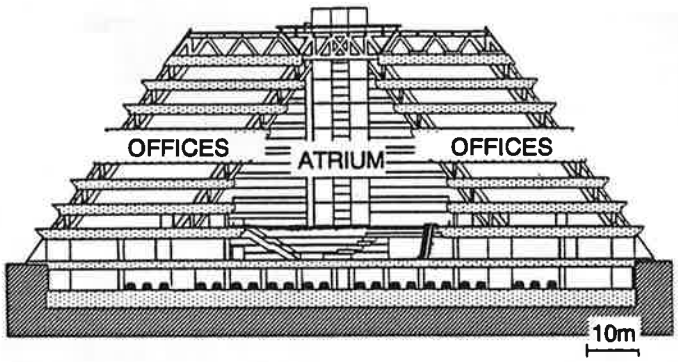

Fig. 26 Atrium between two structures

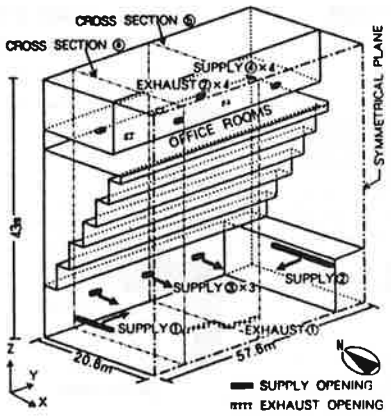

Fig. 27 Model for calculation

i) How much heat from the atrium penetrates into the offices if the window between the atrium and the offices is opened?

ii) How effective is the storage space for hot air at the top of the atrium?

1) Outline of numerical analysis (Figure 26, 27)

As is shown in Figure 26, the atrium is symmetrical; therefore, the numerical analyses were carried out for only half the space of the model, as is shown in Figure 27. The k - ε model was used here also. Furthermore, in order to study the air flow between the atrium and office rooms, a model including only office room space on the eighth floor was also used. The boundary conditions related to temperature include internally generated heat such as that arising from sunshine, lighting and heat penetrating through the walls; hence heat flow

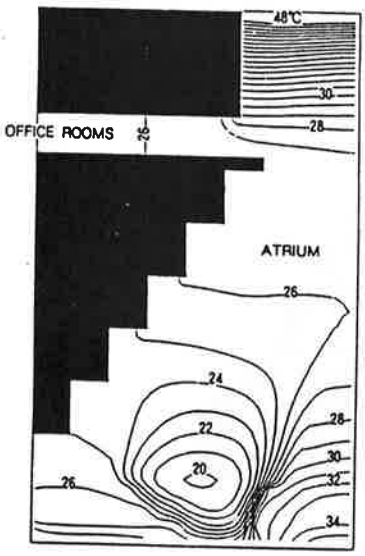

Fig. 28 Temperature distribution under cooling condition (cross section ⓐ)

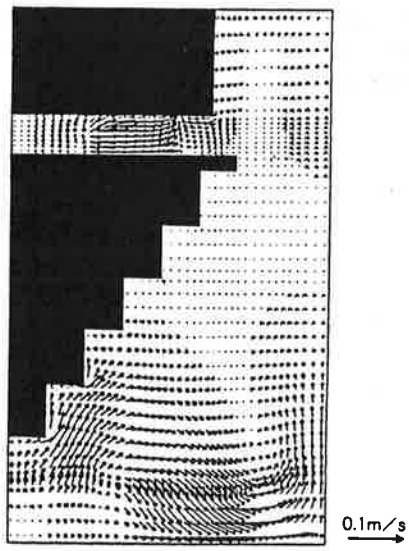

Fig. 29 Air flow distribution under cooling condition (cross section ⓐ)

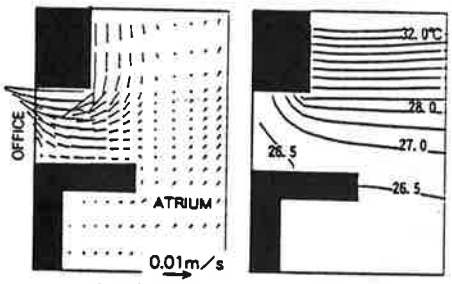

(a) air flow (b) temperature

Fig. 30 Interaction between office and atrium (cross section ⓐ)

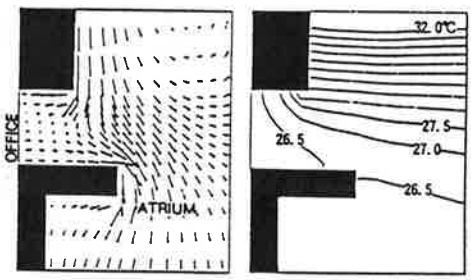

(a) air flow (b) temperature

Fig. 31 Interaction between office and atrium (cross section ⓑ)

through the ceiling, floor and walls was assumed. The total number of grids was 43(X) × 48(Y) × 48(Z)=99072.

2) Temperature distribution under cooling conditions in the atrium (Figure 28)

The temperature near the ceiling of the atrium is high, between 40 and 50 ℃ . However, this high- temperature region remains entirely within the storage space for hot air. At the bottom of the atrium, another high- temperature region, 35 ℃ , is observed in one area. This can be explained by the fact that the width of supply opening ① on the west side is small; thus the cold air does not reach the central region of the atrium.

3) Air flow distribution under cooling conditions in the atrium (Figure 29)

At the upper portion of the atrium, due to the effect of the thermal stratification, the air flow is stagnant. Conversely, at the bottom of the atrium, the flow velocity is relatively high due to the effect of air blown through supply openings and ascending flow is observed caused by a high- temperature region in one part of the bottom of the atrium.

4) Interaction between office and atrium (Figure 30, 31)

The direction of air flow at the border between the office rooms and the atrium differs according to the position of the section. As is shown in Figure 30(a), at cross section ⓐ hot air invades the office rooms from the atrium side. At cross section ⓑ , shown in Figure 31(a), almost identical amounts of air flow in and out of the atrium. This can be explained by the pressure distribution corresponding to the locations of air outlets and inlets in the office rooms.

6.5.3. Case study 3 ; analysis of large atrium covered with glass (Tokyo International Forum, Tokyo, Japan, under construction) [15]

1) Turbulent flow simulation coupled with solar radiation analysis

The numerical simulation system consists of the following three sub- systems:

(1) simulation of air velocity and temperature distributions in enclosure based on the k- ε model;

(2) simulation of radiative heat transfer between the wall boundaries;

(3) simulation of the effects of direct solar radiation, diffused solar radiation and diffused reflection of solar radiation, considering the geometrically complex shape of the enclosure.

2) Specification of the atrium to be analyzed

The atrium space, which is shaped like a big ship with glass walls, is shown in Figure 32. The length, height and width of the space is about 200 m × 65 m × 32 m. The floor area is about 3,300 m^2 and its capacity is about 200,000 m^3. The main zone occupied by people is the sunken space in first floor of this building. It also has decks along the glass walls of each floor and aisles connecting these decks.

There exist six openings, as is shown in Figure 33.

- 1F north side entrance (H 5.0 m × W 30.0 m : 150.0 m^2)
- 1F south side entrance (H 5.0 m × W 30.0 m : 150.0 m^2)
- Roof vent (H 0.5 m × W 50.0 m : 25.0 m^2) × 4 positions

In case 2, the size of the first floor entrance is reduced (H 2.5 m × W 1.0 m : 2.5 m^2). The roof vents are regarded to be opened fully in the summer condition and closed completely in the winter condition.

36 supply openings are arranged at the first floor level.

The conditions of the air supply used in this enclosure are as follows ;

- Supply nozzle : (H 0.5 m × W 0.7 m) × 36 positions (west side 18, east side 18)
- Supply air velocity : 2.13 m/s
- Supply air volume : 96,500 CMH (in total)

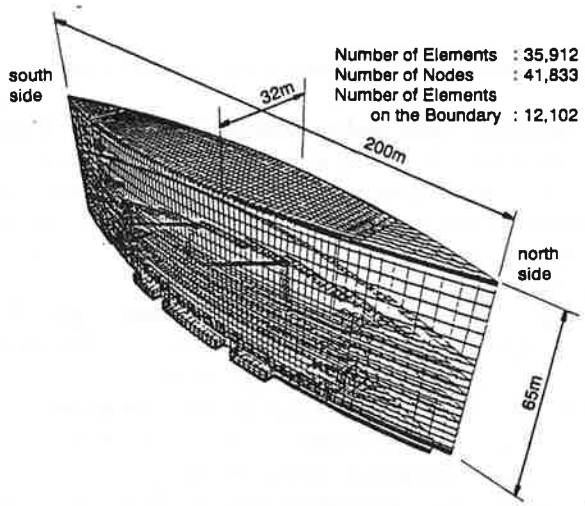

Fig. 32 Shape of atrium and finite element mesh system

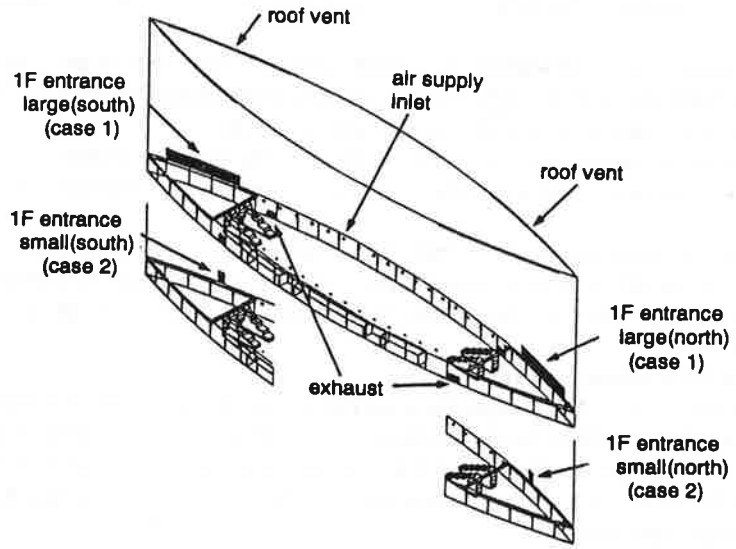

Fig. 33 Entrance (people), air supply and exhaust openings

Fig. 34 Distribution of solar radiation absorbed (case 3)

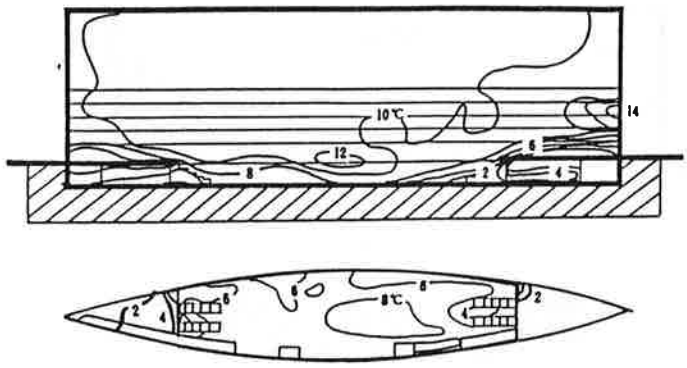

Fig. 35 Temperature distribution under heating condition (case 1)

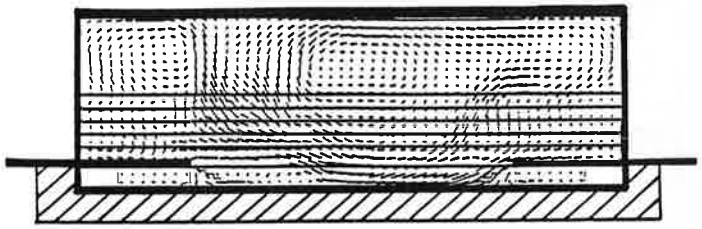

Fig. 36 Airflow distribution under heating condition (case 1)

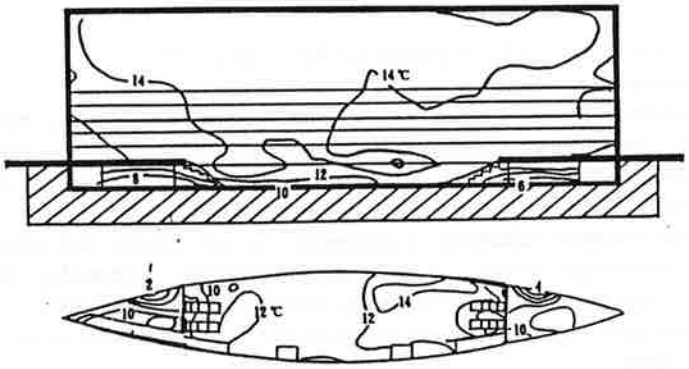

Fig. 37 Temperature distribution under heating condition (case 2)

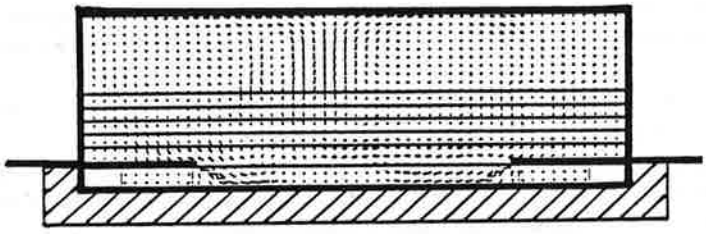

Fig. 38 Airflow distribution under heating condition (case 2)

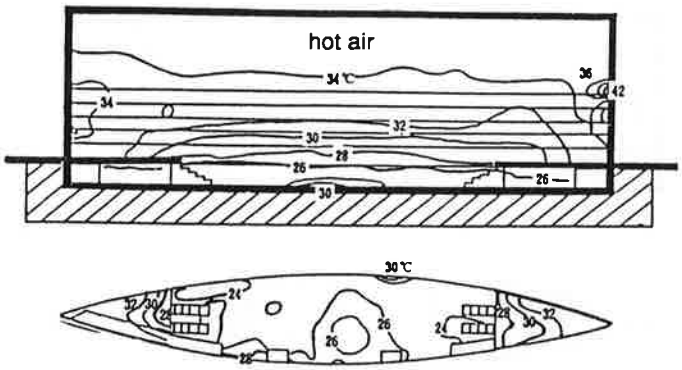

Fig. 39 Temperature distribution under cooling condition (case 3)

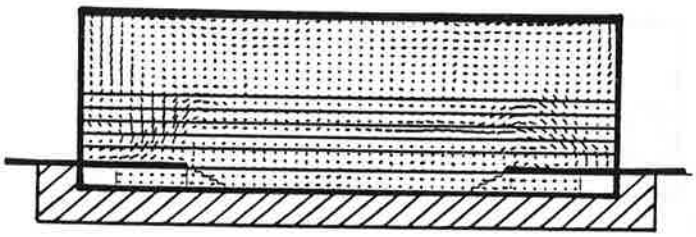

Fig. 40 Airflow distribution under cooling condition (case 3)

• Supply air temperature : 16.0℃ for summer and 30.0℃ for winter

3) Outline of the numerical simulation

This simulation system is composed of the three numerical calculations mentioned above. First the solar radiation absorbed is calculated. The solar radiation absorbed under summer conditions is shown in Figure 34. Next, the radiant heat transfer between the walls is calculated using the quantity obtained in the previous step as the boundary condition.

After the radiation calculation is performed, the air velocity and temperature distribution is simulated based on the $k-\varepsilon$ model using the GSMAC- FEM method [16].

The finite element mesh system used for this calculation is shown in Figure 32.

The indoor space of the enclosure is discretized into 35,912 hexahedral elements.

4) Cases of simulation

11 cases of simulation were conducted. Here, the results of cases 1, 2 and 3 are shown.

In case 1, ventilation is induced by wind pressure under winter heating conditions and the volume of air change at the north side entrance on the 1st floor is given as the boundary condition.

In case 3, ventilation is induced by buoyancy effect under summer cooling conditions, and the inlet air at the roof vents is given as the boundary condition.

In case 2, the entrance opening at the 1st floor is changed to a smaller door opening (H 2.5 m × W 1.0 m : 2.5 m^2). This case is performed to learn the advantage of smaller openings on the 1st floor as opposed to the bigger openings in case 1.

5) Results and discussion

The vertical distributions of temperature and air velocity are presented for a longitudinal cross section taken at the center of the atrium and for a horizontal cross section taken at 1.5m above the floor level. Figures 35~36, Figures 37~38 and Figures 39~40 show these distributions for cases 1, 2 and 3 respectively.

In winter cases (case 1 and case 2), supplied warm air rises due to the buoyancy effect and downward airflow occurs along the glass roof and walls. Consequently large scale recirculating flows are produced in the enclosure. Because of these recirculating flows, the temperature in the enclosure becomes roughly uniform and strong thermal stratification is not observed. Since the cold airflow from the entrance on the first floor descends into the sunken space, the thermal environment there depends upon the volume of the cold airflow. In case 1, the entrance is fully opened, thus the temperature of the sunken space is around 4℃ to 8℃ . On the other hand, the results in case 2 show the temperature of the sunken space as around 10 ℃ to 14 ℃ . Simply by replacing the large openings on the first floor with door openings of smaller size, the thermal environment is improved significantly.

In the summer case (case 3), a recirculating flow cannot be observed in the enclosure, and rather a weak thermal stratification is formed. The cooling airflow from the supply openings at the first floor level descends to the sunken space without mixing with the airflow from the entrance. The temperature of the sunken space is thus around 26 ℃ average, and a rather good environment is obtained.

6. Conclusion

1. There is a general tendency for various outdoor events and activities to be gradually moved indoors. Construction of ever larger enclosures may be expected in the future.
2. The indoor climate control of large enclosures is much more difficult than that of smaller ones such as offices. These difficulties are caused by many factors, including the huge capacity of the space, the great height of the ceiling, and the small zone to be occupied.
3. Before the actual construction of a large enclosure, it is highly desirable that a preliminary assessment of indoor climate based on some type of prediction method be made. Here numerical prediction is very promising.
4. There exist various difficulties in the numerical simulation of a large enclosure, caused mainly by the coarseness of the grid discretization necessitated by the large spaces.

Nomenclature

x_i : three components of spatial coordinate (i = 1,2,3 : streamwise, lateral, vertical)
U_i : three components of average velocity vector
u_i : three components of fluctuating velocity vector
Θ : average value of temperature
θ : fluctuation of temperature
ν_t : eddy viscosity
ν : kinematic viscosity
k : turbulent kinetic energy, $k = \frac{1}{2}\overline{u_i u_i}$
ε : dissipation rate of k
P_k : production of k
$\overline{u_i u_j}$: Reynolds stress
$\overline{u_i \theta}$: turbulent heat flux
$P_{1\varepsilon}$: $P_{1\varepsilon 1} + P_{1\varepsilon 2}$ = production of $\overline{u_i \theta}$ by mean temperature and velocity gradient
τ_W : wall shear stress
ρ : density
$h_1^{(*)}$: distance of first cell from wall
g : gravitational acceleration
β : coefficient of volumetric expansion
K : proportionally constant centerline velocity of jet
σ_ε : 0.9 C_ε : 0.09 E : 9.0 κ : 0.4

Acknowledgements

The analyses of the characteristics of indoor climate in large enclosures were conducted in cooperation with Mr. T. Chikamoto (Univ. of Tokyo)

The numerical studies using the k- ε model, ASM and LES were carried out in cooperation with Professor S. Kato, (Univ. of Tokyo), Dr. A. Mochida (Univ. of Tokyo), Dr. Y. Kondo (Nikken Sekkei Ltd.), Mr. T. Chikamoto and other members. Numerical simulations for case study 2 were conducted by Dr. Y. Kondo and for case study 3 by Mr. T. Saito (Research Center Asahi Glass), Mr. S. Ohgaki (Amenitec) etc. under the guidance of S. Murakami.

This paper was written with the assistance of Mr. T. Chikamoto and Mr. H. Kobayashi (Univ. of Tokyo). The author would like to express his gratitude for their valuable contributions to this work.

Appendix 1 Overestimation of turbulence energy k at frontal corner of building model.

The value of P_k at the center section is estimated. Considering the symmetrical nature of the model and neglecting the small terms, P_k is given as follows:

$$P_k \fallingdotseq \underbrace{-\overline{u_1^2}\frac{\partial U_1}{\partial x_1}-\overline{u_3^2}\frac{\partial U_3}{\partial x_3}}_{P_{k,n}} \underbrace{-\overline{u_1u_3}\frac{\partial U_1}{\partial x_3}-\overline{u_3u_1}\frac{\partial U_3}{\partial x_1}}_{P_{k,s}}, \tag{A.1}$$

where $P_{k,n}$ is the turbulence production by diagonal elements of the strain- rate tensor and $P_{k,s}$ is that produced by off- diagonal elements. The expression for $P_{k,n}$ in eqn.(A.1) can be rewritten using the continuity equation as follows:

$$P_{k,n} \fallingdotseq -(\overline{u_1^2}-\overline{u_3^2})\frac{\partial U_1}{\partial x_1}. \tag{A.2}$$

In the case of $k-\varepsilon$, eqn.(A.2) is transformed into eqn.(A.3) by eddy viscosity modelling.

$$P_{k,n} \fallingdotseq 4\nu_t\left(\frac{\partial U_1}{\partial x_1}\right)^2. \tag{A.3}$$

In general, the magnitude of $P_{k,n}$ does not become so large in the cases of LES and ASM, since $P_{k,n}$ is calculated using the exact form of eqn. (A.2) which is expressed as the subtraction of $\overline{u_1^2}$ and $\overline{u_3^2}$. On the other hand, the turbulence production due to $\overline{u_1^2}$ and $\overline{u_3^2}$ is simply added in the case of $k-\varepsilon$ EVM as expressed by eqn.(A.3), and hence the value of $P_{k,n}$ becomes very large. This is the fallacy inherent in the EVM model. This overestimation of k caused by the diagonal elements of the strain- rate tensor is the fundamental shortcoming of eddy viscosity modelling when it is applied to a flowfield involving stagnation where large values of $\partial U_i/\partial x_i$ usually exist.

The overestimation of $P_{k,s}$ also occurs in the case of $k-\varepsilon$ EVM. The mechanism of overestimation can be shown easily in the same manner as for $P_{k,n}$.

Appendix 2 Difference of evaluation of $\overline{u_i\theta}$ between k − ε model and ASM

The difference of the structure of evaluation of turbulence heat flux $\overline{u_i\theta}$ is tabulated below for the cases of k − ε and ASM.

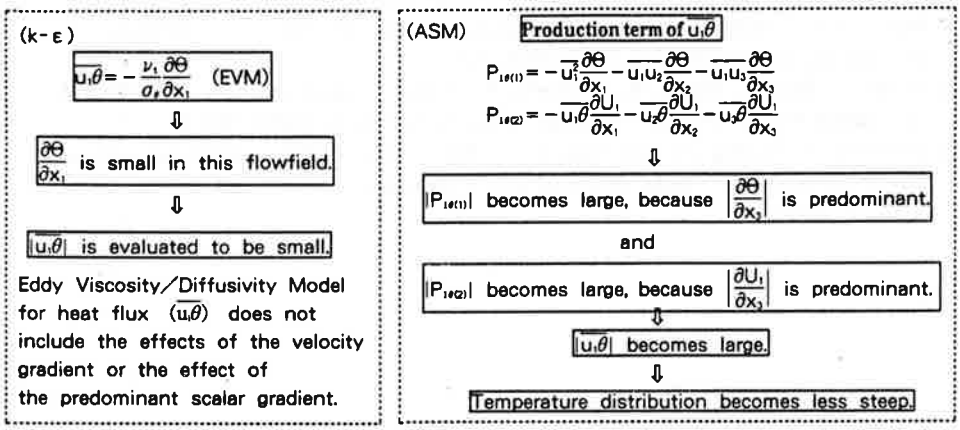

References

[1] Taisei Corp. "X − Seed 4000". (1991)

[2] Obayashi Corp. "Aeropolice 2001". (1991)

[3] Takenaka Corp. Group V 1000 "Sky city 1000, the concept of a vertical composite urban community". (1989)

[4] Kato, S. and Murakami,S. "Model experiment on indoor climate of large-scale space, case study of 15,000 seating capacity sport hall ". Technical Report of Kanto Chapter, AIJ (Architectural Institute of Japan) (1983)

[5] Koestel, A. "Paths of horizontally projected heated and chilled air jets". ASHRAE Transactions, Vol. 61 (1955)

[6] Murakami,S. and Kato, S. "Current status of numerical and experimental methods for analyzing flow field and diffusion field in a room". Building Systems: Room Air and Air Contaminant Distribution, Illinois, ASHRAE (1988.12)

[7] Murakami,S., Mochida,A. and Hayashi,Y. "Scrutinizing k-ε EVM and ASM by means of LES and wind tunnel for flowfield around cube". Eighth Symposium on Turbulent Shear Flows, Munich (1991.9)

[8] Murakami, S., Kato, S. and Kondo,Y. "Numerical prediction of horizontal non-isothermal jet in room based on Algebraic Second-Moment closure model". ASHRAE TRANSACTION Vol. 98 (1992.1)

[9] Murakami, S. and Mochida, A. "3-D numerical simulation of airflow around a cubic model by means of the k-ε model ". J. of Wind Engineering and Industrial Aerodynamics, 31 (1988)

[10] Kato, S., Murakami, S. and Suyama, Y. "Study on diagnostic system for simulation of turbulent flow (part 3)". Technical Report of Kanto Chapter AIJ (1985.1)

[11] Ishida, Y., Murakami, S. and Kato, S. "2-D numerical simulation of turbulent room air flow using fortified Navier Stokes scheme". Annual Meeting of AIJ (1989.10)

[12] Launder, B.E. and Spalding, D.B. "The numerical computation of turbulent flows". Computer methods in applied Mechanics and Engineering 3 (1974)

[13] Chikamoto, T., Murakami, S., Kato, S., Mochida, A. and Kondo, Y. "Numerical simulation on velocity and temperature field of large scale indoor space (part 2)". Annual Meeting of AIJ (1990.10)

[14] Kondo, Y., Murakami, S. and Kato, S. "Numerical simulation on flow and temperature fields of large-scale indoor space". The Fourth International Conference on Computing in Civil and Building Engineering, Tokyo (1991.7)

[15] Ohgaki, S., Saito, T., Sonda, Y., and Ozeki, Y. "Analysis on temperature and flow field in the atrium(Part 9)". Annual Meeting of AIJ (going to be published in 1992.8)

[16] Tanahashi, T., Okanaga, H. and Saito, T. "GSMAC finite element method for unsteady incompressible Navier-Stokes equations at high Reynolds number". Int. J. Num. Meth. Fluids, 11 (1990)